Synthesis and Light Emission from ZnO-Coated Silicon Nanorods

Hyunsu Kim, Changhyun Jin, Sunghoon Park, Hyoun Woo Kim,[†] and Chongmu Lee[*]

Department of Materials science and Engineering, Inha University, Incheon 402-751, Korea. [*]E-mail: cmlee@inha.ac.kr
[†]Division of Materials Science and Engineering, Hanyang University, Seoul 133-791, Korea

We report the synthesis and thermal annealing of Si-core/ZnO-shell nanorods using a two-step process comprising the metal-assisted electroless etching of Si and the sputter deposition of ZnO. Transmission electron microscopy and X-ray diffraction analysis showed that the cores of the annealed core-shell nanorods were single crystal diamond cubic-type Si, whereas the shells of the annealed core-shell nanorods were single crystal wurtzite-type ZnO. The PL spectra of Si nanorods consisted of a broad red emission band and a weaker blue emission band. The major emission band of Si nanorods was shifted from 700 nm (in the red region) to 440 nm (in the violet region) by ZnO coating. The violet emission of the core-shell nanorods was enhanced in intensity considerably by annealing in an oxidizing atmosphere. The origin of the PL enhancement by annealing is also discussed.

Key Words : Si-core/ZnO-shell nanorods, Electroless etching, Sputter deposition, Photoluminescence, Thermal annealing

Introduction

In recent years, one dimensional (1D) silicon nanostructures have attracted significant attention mainly due to their unique optical properties and their ability to emit visible light as well as the central role of silicon in the semiconductor industry. 1D silicon nanostructures have the potential to be used for next-generation high integrated electronic devices. 1D silicon nanostructure field effect transistors may exhibit promising transport characteristics compared to the devices fabricated by top-down approaches.[1,2] 1D silicon nanostructures also find applications in optoelectronics and chemical and biological sensors.[3-5] Many techniques such as masking, lithography, metal-catalytic vapor-liquid-solid (VLS) method, oxide assisted metal catalyst-free method, and solution techniques have been developed to fabricate 1D silicon nanostructures.[6,7] These methods yield nanowires with different orientations and diameters.

It is desirable to passivate the surface of one-dimensional (1D) nanostructures to control the surface reactivity and to lower the surface state density. A common technique to control and enhance the properties of 1D nanostructures is to create core-shell heterostructures by sheathing them with other materials.[8-10] We can also give nanostructures various functions that can be used effectively for nanoscale electronic or optoelectronic devices by making core-shell nanostructures.[11-13] For example, the PL emission intensity of the light emitted from nanostructures can be significantly increased or the wavelength of the emission can be controlled by sheathing them with a proper material with the optimal layer thickness.[14-18] There have been many reports on the core-shell 1D nanostructures with Si cores but very few reports on Si-core/ZnO-shell1D nanostructures to date. Very recently, Sun *et al.*[19] reported the synthesis, structure, and photoluminescence (PL) properties of Si-core/ZnO-shell nanowire arrays and porous Si-core/ZnO-shell nanowire arrays. However, the influence of annealing on the PL properties of these nanostructures has not been reported yet. In this paper, we report the synthesis, structure, and PL properties of Si-core/ZnO-shell nanorods synthesized by a two-step process comprising the metal-assisted electroless etching of Si and the sputter-deposition of ZnO and examined the influence of annealing on the PL properties of these nanostructures in an oxidizing atmosphere.

Experiments

Si-core/ZnO-shell nanorods were synthesized by using a two-step process comprising the metal-assisted electroless etching of Si and the sputter deposition of ZnO. First, Si (100) wafer pieces were cleaned by sonication in acetone followed by rinsing in isopropyl alcohol and then the substrates were dipped in a HF solution (H_2O:HF = 3:1) to remove the native oxides on the Si wafer for 2 min. The cleaned substrates were etched in an aqueous $AgNO_3$ solution (H_2O:$AgNO_3$: HF = 43:12:5) at 60 °C for 2 h. Upon removal from the etch bath, the thin Ag layer deposited on top of the nanorod arrays was dissolved by dipping the wafer pieces in nitric acid.

Si-core/ZnO-shell nanorods were prepared by the sputter-deposition of ZnO thin films on the Si nanowire samples in a radio frequency (rf) magnetron sputtering system at room temperature. After the vacuum chamber was evacuated to 1×10^{-6} torr using a turbomolecular pump backed by a rotary pump. Depositions were carried out at a system pressure of 1.8×10^{-2} Torr and an rf power of 100 W in an argon (Ar) atmosphere. The Ar gas flow rate was 30 standard cubic centimeters per minute (sccm). Subsequently, the prepared

core-shell nanorod samples were annealed at 600 °C for 30 min in an O_2 atmosphere.

The products were then characterized using glancing angle (0.5°) XRD (X'pert MPD-Philips with Cu-Kα radiation), field emission scanning electron microscopy (FESEM, Hitachi S-4200), and TEM (Phillips CM-200). The high resolution TEM (HRTEM) images and selected area electron diffraction (SAED) patterns were also taken on the same TEM system at an acceleration voltage of 200 kV. The compositional analysis was done by using energy dispersive X-ray spectroscope (EDXS) installed in the TEM. The PL measurements were carried out at room temperature in a PL spectrometer (Kimon, SPEC-14031K, Japan) with a He-Cd laser line of 325 nm as the excitation source.

Results and Discussion

Figure 1(a) and (b) show the FESEM image of the Si nanorod array and the Si-core/ZnO-shell nanorod array synthesized in this study. No distinct difference is not noted between the two different kinds of nanorod arrays in the SEM image. The nanorods were vertically oriented in the form of bundles. The diameters of the core-shell nanorods range from 80 to 120 nm, and the average length is ~10 μm. The glancing-angle XRD patterns of the as-synthesized and annealed core-shell nanorods are shown in Figure 2(a) and (b), respectively. The reflection peaks for both the as-synthesized and annealed nanorods are readily indexed to the diamond cubic structure of Si with lattice constants of a = 0.543 nm (JCPDS 27-1402) and the wurtzite structure of ZnO (JCPDS 79-0206, P63mc, a = 0.3249 nm, c = 0.5206 nm), which confirms that the nanorods consist of crystalline Si cores and crystalline ZnO shells. The pattern exhibits the (111), (220), (311), and (400) peaks characteristic of Si and five other peaks characteristic of wurtzite-type ZnO which are indexed as the (100), (002), (101), (103), and (112) reflections from ZnO. The ZnO reflection intensity peaks for the as-synthesized nanorods are much lower than those for the annealed ones, suggesting that the crystallinity of the ZnO shells have been enhanced by thermal annealing.

Figure 3 shows a low-magnification TEM image of a typical Si-core/ZnO-shell nanorod clearly indicating that there are two segments in the structure: a rod-like core and two thin coating layers on both edge sides of the nanorod. Figure 4 is the lattice-resolved high-magnification TEM
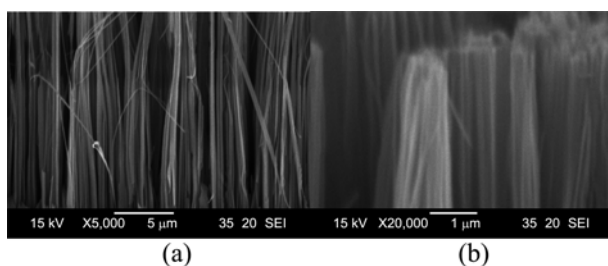

Figure 1. SEM images of (a) the Si nanorod array and (b) the Si-core/ZnO-shell nanorod array synthesized on the Si (100) substrate.
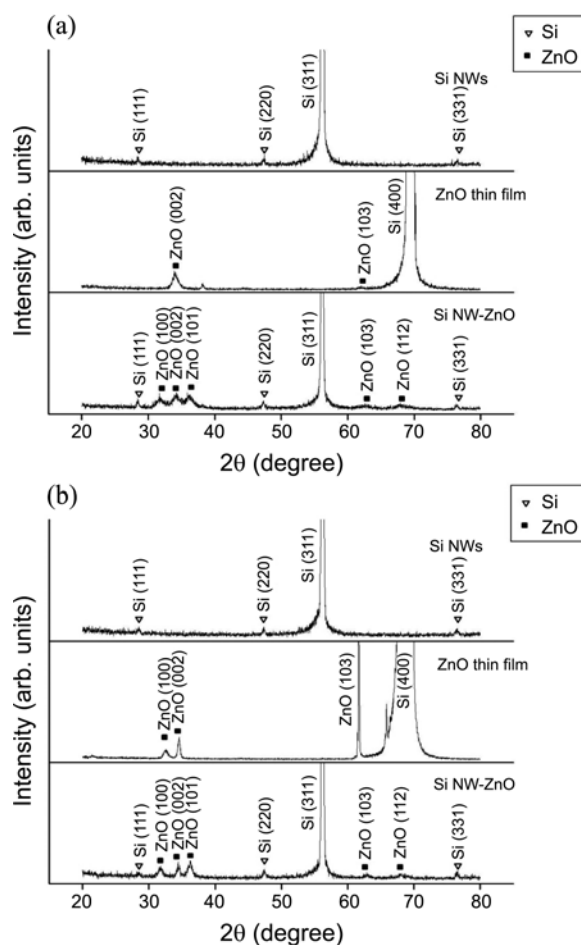

Figure 2. XRD patterns of the Si-core/ZnO-shell nanorods: (a) as-synthesized and (b) annealed.

image of the annealed core-shell nanorod, respectively. The single crystalline nature of the core in the nanorod can be identified from the corresponding SAED pattern in the inset
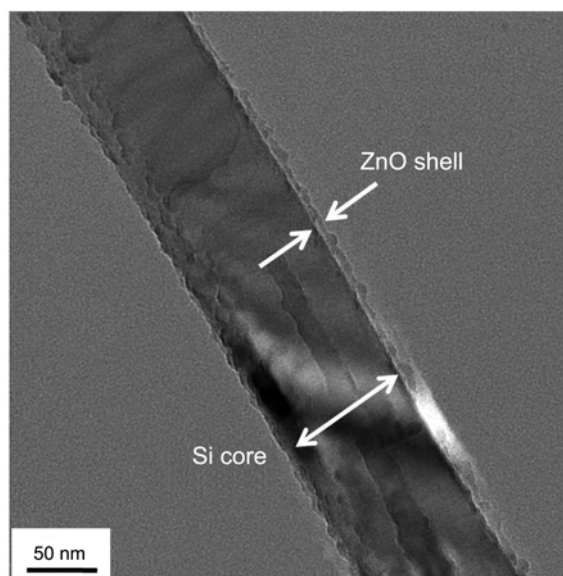

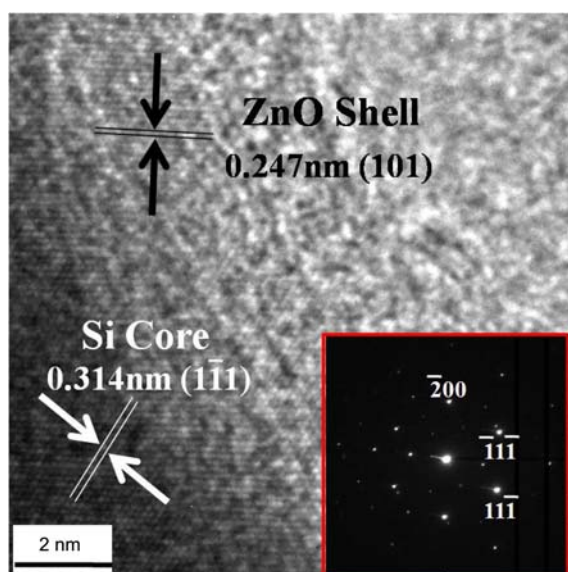**Figure 3.** Low-magnification TEM image of a typical Si-core/ZnO-shell nanorod.

Figure 4. HRTEM image of a typical Si-core/ZnO-shell nanorod. Inset, corresponding SAED pattern.

of Figure 4. Besides a set of strong spotty pattern, a set of weak spotty pattern for wurtzite-type ZnO are observed as well. The weak spotty pattern for the ZnO shell reflects the far smaller thickness of the shell compared with that of the core. The zone axis of the strong spotty pattern is indexed to be the [011] direction of the Si core with the face-centered cubic (fcc) structure. The interplanar spacings corresponding to the {1$\bar{1}$1} plane family of the Si core and the {101} plane family of the ZnO shell are 0.314 and 0.247 nm, respectively.

As regards the PL of 1D silicon nanostructures, it is known to be weak and complicated. Unlike bulk Si, a 1D silicon nanostructure can become a direct bandgap semiconductor at nanometer diameter.[20,21] Several researchers have reported the PL from the 1D silicon nanostructures of as-grown and oxidized samples at room temperature.[7,22-28] Multiple bands have been observed, spanning from near-infrared to ultraviolet wavelengths, and tentatively assigned to contaminated or defective Si oxide, dangling bonds, and quantum confinement effects. For example, a fairly broad red emission band centered at around 700 nm and a weaker blue band at about 480 nm from oxide-assisted SiNWs were reported.[7,22] A broad PL emission peaked at 750 nm was reported for 1D silicon nanostructures 50 nm wide.[23] There is also a report on a green-blue emission band at around 605 nm with a shoulder at 729 nm in the red region from the oxide-assisted grown 1D silicon nanostructures with diameters in a range from a few to a few tens of nanometers.[24] The observed green-blue emission was ascribed to recombination in the oxide shell whereas the red emission from nanocrystalline Si was related to quantum confinement effects, respectively. Bai *et al.* however, noted that confinement-related emission should be negligible if the 1D silicon nanostructure diameter is larger than the Bohr radius in Si (~5 nm).[28] They proposed that structural defects such as stacking faults and twin boundaries are responsible for the red fluorescence.
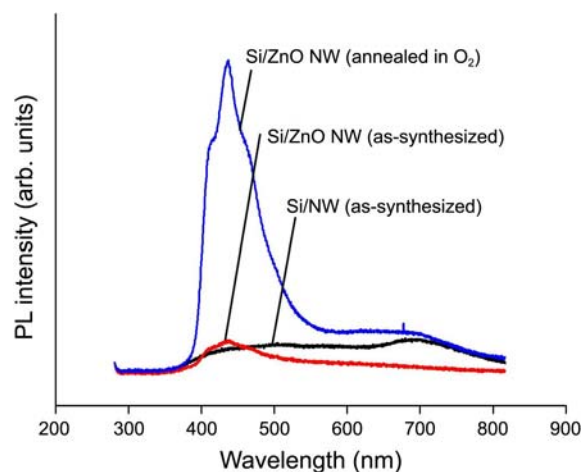

Figure 5. Influence of the annealing atmosphere on the PL of Si-core/ZnO-shell nanorods (1500 ALD cycles). The nanorod samples were annealed at 600 °C for 30 min in different atmospheres.

Figure 5 compares the PL spectra of Si nanorods before and after ZnO coating. The PL spectra of Si nanorods consist of a fairly broad red emission band centered at around 700 nm and a weaker blue emission band centered at around 500 nm. These results are in good agreement with recent reports on similar 1D silicon nanostructures.[7,22] In contrast, the Si-core/ZnO-shell nanorods had a major emission band at around 440 nm in the violet region. Figure 6 shows the normalized PL spectrum of the as-synthesized core-shell nanorods. Gaussian fitting analysis revealed that of the emission of the core-shell nanorods is composed of three recognizable emission bands centered at 415 nm in the violet region, 487 nm in the blue region, and 608 nm in the orange region, respectively. The origins of the emissions from our Si/ZnO core-shell nanorods, in particular, the origin of the violet emission from the core-shell nanorods are not well understood at this moment, but they are assumed to be attributed to the recombination from the defect centers such as O and Zn interstitials, Si suboxides, stacking faults, twin boundaries rather than to the quantum confinement effect since our nanorod diameters are too large (~100 nm) for
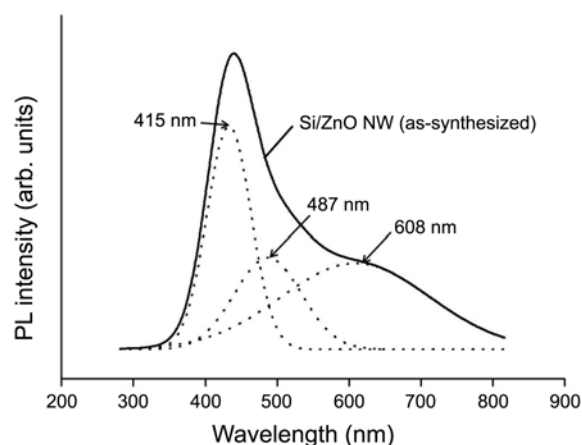

Figure 6. Normalized PL spectrum of Si nanorods. The spectrum exhibits the three-peak Gaussian fitting.
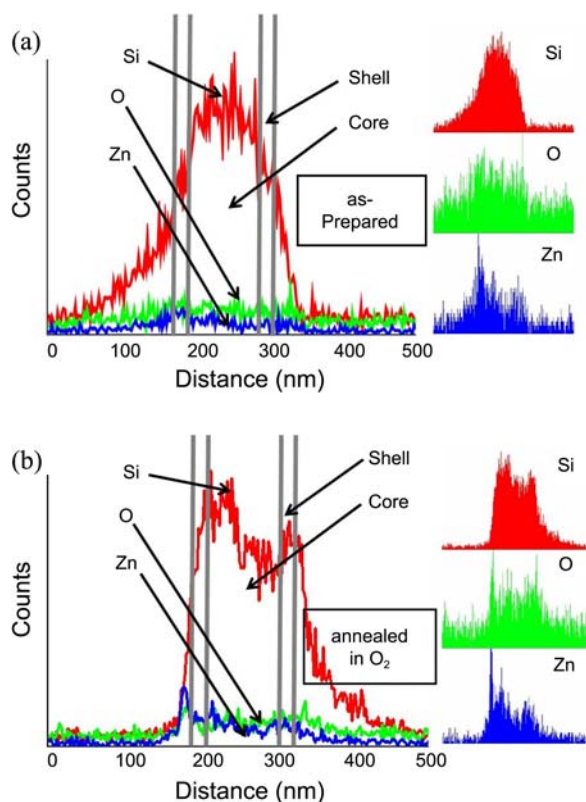
Figure 7. EDXS line scanning concentration profiles of the Si-core/ZnO-shell nanorods (a) as-synthesized and (b) annealed in an O₂ atmosphere at 600 °C for 30 min.

Figure 8. EDXS elemental maps of the Si-core/ZnO-shell nanorods: (a) as-prepared, and (b) annealed in an O₂ atmosphere at 600 °C for 30 min.

quantum confinement effect.

Figure 5 also shows that the violet emission is significantly enhanced in intensity by thermal annealing in an oxidizing atmosphere. EDXS analysis was performed to examin the origin of the PL enhancement by annealing in an oxidizing atmosphere. The line-scanning EDXS concentration profiles in Figure 7(a) and (b) show the distribution of Si, Zn, and O elements along the diameter of a typical nanorod in the Si/ZnO core-shell nanorod samples as-synthesized and annealed in an oxidizing atmosphere, respectively. Comparison of Figure 6(a) and (b) gives that the oxygen and zinc concentrations in the core-shell nanorod sample annealed in an oxidizing atmosphere (Fig. 7(b)) are evidently higher than those in the as-synthesized nanorod sample (Fig. 7(a)). Comparison of the EDXS element maps in Figure 8(a) and (b) confirms this fact. The higher density of blue spots (the O elements) in the nanorod in Figure 8(b) than in Figure 8(a) indicates the increase in the O concentration in the nanorod by annealing. These results suggest that the concentrations of the oxygen interatitials, *i.e.*, Si suboxides as well as the Zn interstitials in the Si cores were increased by the diffusion of zinc and oxygen from the ZnO shell and the oxidizing atmosphere to the Si core during the annealing process, which presumably led to the enhancement of the violet emission in intensity.

There is also a possibility of the Si nanorods to be turned to SiO_x through the O₂ annealing treatment, which might cause the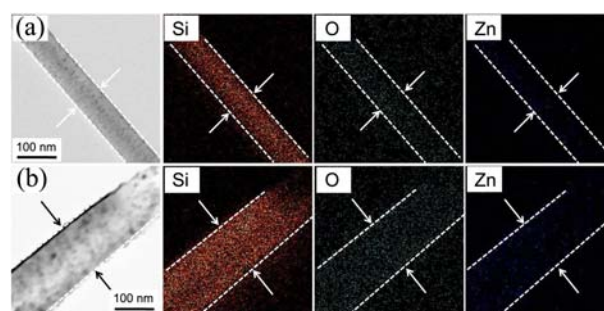 changes of the emission in UV-blue region. It was reported previously that Si/SiOₓ core-shell nanorods have a stable and strong blue emission, and its ultraviolet light emission (415 nm) is attributed to two-fold coordinated silicon lone-pair centers.[29] From this point of view, violet light emission of Si/ZnO nanorod annealed in O₂ could be also attributed to the formation of SiO_x after O₂ annealing.

Conclusions

Si-core/ZnO-shell coaxial nanorods were successfully synthesized by using a two-step process: the metal-assisted electroless etching of silicon and the sputter-deposition of ZnO. The cores of the annealed core-shell nanorods were single crystal diamond cubic-type Si, whereas the shells of the annealed core-shell nanorods were single crystal wurtzite-type ZnO. The PL spectrum of Si nanorods consists of a fairly broad red emission band centered at around 700 nm and a weaker blue emission band centered at around 500 nm. In contrast, the Si-core/ZnO-shell nanorods have a major violet emission band at around 440 nm. The violet emission of the core-shell nanorods is significantly enhanced in intensity by annealing in an oxidizing atmosphere. The emission enhancement by annealing in an oxidizing atmosphere is mainly attributed to the increase in the O and Zn interstitial concentrations in the Si cores and formation of SiO_x layer.

References

1. Duan, X.; Niu, C.; Sahi, V.; Chen, J.; Parce, J. W.; Empedocles, S.; Goldman, J. L. *Nature* **2003**, *425*, 274.
2. Cui, Y.; Zhong, Z.; Wang, D.; Wang, W. U.; Lieber, C. M. *Nano Lett.* **2003**, *3*, 149.
3. Cullis, A. G.; Canham, L. T. *Nature* **1991**, *353*, 335.
4. Lin, V. S. Y.; Motesharei, K.; Dancil, K. P. S.; Sailor, M. J.; Ghadiri, M. R. *Science* **1997**, *278*, 840.
5. Stewart, M. P.; Buriak, J. M. *Adv. Mater.* **2000**, *12*, 859.
6. Marsen, B.; Sattler, K. *Phys. Rev. B* **1999**, *60*, 11593.
7. Ma, D. D. D.; Lee, C. S.; Au, F. C. K.; Tong, S. Y.; Lee, S. T. *Science* **2003**, *299*, 1874.
8. Morales, A. M.; Lieber, C. M. *Science* **1998**, *279*, 208.
9. Kim, N. H.; Kim, H. W.; Seoul, C.; Lee, C. *Mater. Sci. Eng. B*

2004, *111*, 131.

10. Wu, Y.; Xiang, J.; Yang, C.; Lu, W.; Lieber, C. M. *Nature* **2004**, *430*, 61.

11. Lauhon, L. J.; Gudiksen, M. S.; Wang, D.; Lieber, C. M. *Epitaxial Nature* **2002**, *420*, 57.

12. Choi, H. J.; Johnson, J. C.; He, R.; Lee, S. K.; Kim, F.; Pauzauskie, P.; Goldberger, J.; Saykally, R. J.; Yang, P. *J. Phys. Chem. B* **2003**, *107*, 8721.

13. Kim, H. W.; Shim, S. H.; Lee, C. *Mater. Sci. Eng. B* **2007**, *136*, 148.

14. Park, S.; Kim, H.; Lee, J. W.; Kim, H. W.; Lee, C. *J. Kor. Phys.* **2008**, *53*, 657.

15. Kim, H. W.; Lee, J. W.; Kebede, M. A.; Kim, H. S.; Srinivasa, B.; Kong, M. H.; Lee, C. *J. Nanosci. Nanotechnol.* **2008**, *8*, 5715.

16. Park, S.; Jun, J.; Kim, H. W.; Lee, C. *Solid State Commun.* **2009**, *149*, 315.

17. Jun, J.; Jin, C.; Kim, H.; Kang, J.; Lee, C. *Appl. Phys. A* **2009**, *96*, 813.

18. Jin, C.; Kim, H.; Kim, H. W.; Lee, C. *J. Lumin.* **2010**, *130*, 516.

19. Sun, L.; He, H.; Liu, C.; Lu, Y.; Ye, Z. *Cryst. Eng. Comm.* **2011**, *13*, 2439.

20. Ma, D. D. D.; Lee, S. T.; Shinar, J. *Appl. Phys. Lett.* **2005**, *87*, 033107.

21. Canham, L. T. *Appl. Phys. Lett.* **1990**, *57*, 1046.

22. Lehmann, V.; Gosele, U. *Appl. Phys. Lett.* **1991**, *58*, 856.

23. Dovrat, M.; Arad, N.; Zhang, X. H.; Lee, S. T.; Sa'ar, A. *Phys. Stat. Sol. (a)* **2007**, *204*, 1512.

24. Lee, S. T.; Wang, N.; Lee, C. S. *Mater. Sci. Eng. A* **2000**, *286*, 16.

25. Colli, A.; Hoffman, S.; Fasoli, A.; Ferrari, A. C.; Ducati, C.; Dunin-Borkowski, R. E.; Robertson, J. *Appl. Phys. A* **2006**, *85*, 247.

26. Wu, C.; Qin, W.; Qin, G.; Zhao, D.; Zhang, J.; Xu, W.; Lin, H. *Chem. Phys. Lett.* **2003**, *378*, 368.

27. Koch, F.; Petrova-Koch, V.; Muschik, T. *J. Lumin.* **1993**, *57*, 271.

28. Fauchet, P. M. *J. Lumin.* **1996**, *70*, 294.

29. Itoh, C.; Suzuki, T.; Itoh, N. *Phys. Rev.* **1989**, *41*, 3794.